International Journal for Housing Science and Its Applications
Publish August 6, 2025. Volume 46, Issue 3 Pages 4784-4795

https://doi.org/10.70517/ijhsa463409

Study of permafrost changes in the upper Irtysh River basin driven by meteorological data based on nonlinear analysis method

Ting Kong[1], Shuai Li[2], Pu Zhang[1,*], Qinglei Li[3], Weiping Liu[1] and Qiwen Wang[1]
[1] Xinjiang Meteorological Information Center, Urumqi, Xinjiang, 830002, China
[2] The Lightning Protection Center of Xinjiang Uygur Autonomous Region, Urumqi, Xinjiang, 830002, China
[3] National Meteorological Information Center, Beijing, 100081, China

Corresponding authors: (e-mail: 18963817495@sohu.com).

Abstract In recent years, degradation of perennial permafrost has occurred against the background of a clear warming trend. Therefore, it is of great scientific significance to carry out research on permafrost changes and hydrological response under multi-year climate change conditions. Taking the Irtysh River Basin as the study area, this paper explores the connection between perennial permafrost changes and climate by taking multi-year meteorological data as the support and adopting SHAWDHM, a distributed hydrological model coupled with a permafrost module, to simulate the upstream sub-watersheds of the headwater area of the Irtysh River Basin. At the same time, we analyzed the permafrost hydrological change pattern of the upper watershed of the Irtysh River basin from 1968 to 2022, and simulated the year-by-year changes of soil infiltration, measured 20% annual precipitation, and the proportional relationship of the area of perennial permafrost to the total area of the watershed. The planar distribution of perennial permafrost degraded significantly from 1990 to 2022, and the newly added and degraded permafrost were located in the area where seasonal permafrost was in transition to perennial permafrost. The proportion of perennial permafrost area fluctuates above and below 35% from 1972 to 1996, and the change of soil infiltration obtained by simulation is mainly affected by the change of precipitation. And after 2008, with the increase of temperature, the soil hydraulic conductivity increases, and the soil infiltration volume rises rapidly when the increase of precipitation is not significant.

Index Terms SHAWDHM model, meteorological data, permafrost, hydrological changes, Irtysh River

I. Introduction

The effect of global warming on perennial permafrost is one of the major impacts of global change, and the study of the impact of the resulting permafrost changes on runoff is currently a hot area of hydrological research in cold regions [1], [2]. The Irtysh River is the only transboundary river in China that flows into the Arctic Ocean from east to west, and the strategic position of the Altai region, where the river is located, is particularly important as the northern corridor of the Silk Road Economic Belt and an important node city for Xinjiang to participate in the construction of the China-Mongolia-Russia Economic Corridor [3]. Climate warming over the past decades has induced extensive changes in regional permafrost, and such changes have led to responses of increased winter runoff from rivers [4], [5]. Therefore, the study of hydrologic effects of perennial permafrost changes in this region is important for predicting future runoff changes in the region.

The presence of permafrost as an impermeable layer can have a direct effect on the watershed runoff process, resulting in a larger direct surface runoff and a smaller subsurface runoff, which results in a larger peak river runoff [6]. In contrast, the baseflow runoff is smaller in winter, showing a better relationship between the perennial permafrost cover of the watershed and the ratio of maximum and minimum monthly runoff in the watershed [7]. Meanwhile, the change or disappearance of the active layer of perennial permafrost will directly control the change of groundwater level in the perennial permafrost zone, and this change of the active layer will directly affect the surface ecological processes [8], [9]. In addition, the presence of permafrost in the watershed also inhibits the evaporation process to some extent [10]. Winter runoff of some rivers with perennial permafrost distribution in western and northeastern China also showed an increasing trend, such as the winter runoff of the Kriya River in the Kunlun Mountains of Xinjiang, the Manas River in the Tianshan Mountains, the Lhasa River in Tibet, and the upper reaches of the Songhua River in northeastern China [11]-[14]. The increasing trend of winter runoff in the above mentioned perennial permafrost-distributed rivers may be caused by perennial permafrost degradation, i.e., permafrost degradation makes the water-insulating effect of the perennial permafrost disappear, which results in

more surface water recharge to groundwater [15]-[17]. The simulation results of the impact of multi-year permafrost change scenarios on groundwater runoff also indicate that multi-year permafrost degradation will increase groundwater runoff in successive years of permafrost zones [18]. However, there is a lack of effective monitoring of permafrost degradation at the basin scale, which makes it difficult to give a direct indication of the effect of multiyear permafrost degradation on runoff [19], [20]. On the other hand, the upper part of the Irtysh River basin is a typical semi-arid cold region basin, and the permafrost changes in this basin need to be further revealed.

This paper analyzes the geographic location, topography, meteorological characteristics of the study area (Irtysh River Basin) and the actual conditions of the sub-basins upstream of the source area of the Irtysh River Basin. The freezing number model based on empirical statistics is selected to analyze the distribution of permafrost in the Irtysh River basin. Given the advantages of the SHAWDHM model, the SHAWDHM model was used to simulate and analyze the hydrological changes of permafrost in the upstream of the source area of the Irtysh River Basin. Specify the input data as well as the output data of the SHAWDHM model. Three indicators, namely, the proportion of perennial permafrost area, the thickness of perennial permafrost active layer, and the maximum freezing depth of seasonal permafrost, were selected to measure the degradation level of permafrost in the basin. Combined with the changing characteristics of permafrost in the Irtysh River basin, the SHAWDHM model was used to simulate the relationship between soil infiltration, measured 20% annual precipitation, and the proportion of perennial permafrost area to the total area of the basin from year to year.

II. Overview of the study area

II. A. Geographical location

The total length of the Irtysh River is about 4,248km, with a basin area of 1,643,000 km^2. The Irtysh River basin is located in the northern part of the Xinjiang Uygur Autonomous Region, with an area of 45,300,000 km^2, and a length of about 630km. the eastern and northeastern part of the basin borders with the People's Republic of Mongolia, the northwestern part with the Republic of Kazakhstan, and the northern part of the basin, at the source of the Burezin River, borders with Russia. the basin has a total length of about 4,248km, with a total length of about 630km.

II. B. Topography and geomorphology

The Altai Mountains are high in the west and low in the east, with the average elevation of the ridgeline dropping from 3,000 meters to about 2,600 meters from west to east.

The Junggar Basin in the south has an elevation of 500m-1000m.

Altai Mountain area is obvious vertical zonal distribution law, according to the vegetation characteristics and conditions of the subsurface can be divided into seven natural geographic zones:

(1) glacier permanent snow belt: located at an altitude of 3200m above sea level, is the glacial action of the alpine zone, snow all year round, constituting the source of the river. Below the snow line, lichens, mosses and sparse hardy plants mainly grow.

(2) Alpine grassland zone: located between 2500m-3200m above sea level, is the ice edge of the role of the high and mid-mountain belt, the annual precipitation of 500mm. by rain, snow erosion, coarse gravel or bare rock is mainly, there is permafrost layer, soil is mainly alpine meadow soil, plant growth is not high, mainly some cold-resistant grasses, the degree of vegetation cover of about 60%.

(3) Sub-alpine forest and grassland belt: Located between 2000m-2500m above sea level, it is a mid-alpine belt under the action of flowing water, with forests on the shady slopes and scrubs and grasslands on the sunny slopes. The annual precipitation is between 500 mm and 600 mm, and there are many varieties of grasses, which are the main summer pastures in the area. The vegetation cover reaches 70%-80%, and the soil mainly consists of brown calcium soil and chestnut calcium soil.

(4) Central Mountain Grassland Belt: Located between 1500m-2000m above sea level, with annual precipitation of 350mm-500mm, it has dense secondary forests in river valleys, and the vegetation coverage of the sunny slopes is gradually decreasing.

(5) Mountain grassland zone: mainly low hills, located between 900m-1500m above sea level, annual precipitation between 250mm-350mm, in the “inverse temperate zone”, deep snow, herbaceous plant species are rich in shady and sunny slopes with vegetation coverage of 20%-50%, which is the main spring and fall pastures in the area. The mountainous and mesic grassland zone is dominated by the type of arid denudation, and there are more broken and sunken basins and deeply covered Quaternary sediments.

(6) Semi-desert grassland zone: located in the pre-mountainous hilly zone, with an altitude of 700m-900m, annual precipitation of 150mm-250mm, and the transition of plant type to desert vegetation, it can only be used as winter pasture, and it is also the main plantation development area in the locality.

(7) Semi-desert grassland area: located in the alluvial sedimentary plain area in front of the mountains, with an elevation of 500m-700m, presenting a desert landscape type. The soil is mainly stony gobi, gray-brown desert soil and saline soil. The annual precipitation is about 100mm. The vegetation is sparse and short, with perennial drought-tolerant plants dominating. The grass layer is generally 15cm-20cm in height, with a coverage of 8%-10% (desert Gobi areas are also included).

II. C.Meteorological characteristics

(1) Climatic characteristics

E River basin is located in the hinterland of the Eurasian continent, belonging to the continental north temperate and cold temperate climate. The terrain of the basin gradually decreases from northeast to southwest, and it can be divided into three bands of mountainous areas above 1400m, low hills of 700m-1400m and Junggar plains below 700m according to the altitude.

In general, the basin climate characteristics of high latitude, low temperature, less heat, more cold, and winter, spring often accompanied by cold waves, winter and summer temperature difference, the temperature difference between the year is large. Due to the Gobi sandy subsurface temperature by light changes drastically, the day difference is also obvious. Altai mountainous areas have a wetter climate, the southern plains by the Junggar Basin and the Gurbantunggut Desert, the climate is dry and less precipitation. Among the four seasons, spring and fall are not obvious, and can be roughly divided into cold half a year and warm half a year.

(2) Light and Temperature

The basin is located in the northernmost part of Xinjiang, with low solar altitude angle, little heat, and significant differences in air temperature influenced by the vertical and latitudinal zonation of the basin. According to the statistics of 10 meteorological stations in Altay area, the average temperature for many years is 3.2°C, with temperatures between -2°C and -4°C in mountainous areas and about 4°C in plain areas. The highest and lowest extreme temperatures can reach +40°C and -40.8°C, with a historical occurrence of -51°C in CocoThai, one of the lowest records in the country.

(3) Precipitation and Evaporation

Water vapor blowing from the Atlantic and Arctic Oceans enters the Altai region from two places. One, from the west along the Irtysh River. The second, from the lower mountains of the Tacheng area through the Hefeng County.

Abundant water vapor and Altay Mountain oblique convergence, water vapor layer blocked, but also by the topography of the lift, the formation of precipitation on the windward slope, so the mountainous areas of precipitation is more abundant, there is an “inland wet island,” the name.

Altay region belongs to the arid region, less precipitation and strong evaporation, water balance is extremely unbalanced, from the mountains to the plains evaporation with the decrease in elevation and increase. Years of average evaporation (20cm evaporation dish observation value) of the northern hilly areas for 1500mm to 1700mm, the plains up to 1800mm or more.

II. D.Upper Irtysh River

The Irtysh River Basin, which originates on the southern slope of the middle Altai Mountains, is the second largest river in Xinjiang and an international river in the Arctic Ocean water system. Influenced by the westerly wind belt, it receives abundant precipitation and is an important stable snow accumulation area. The spring snowmelt runoff provides sufficient water resources for Altay and its surrounding areas, and its contribution to the basin's water resources should not be overlooked.

Kayiltse River Basin belongs to the upstream sub-basin of the source area of the Erqis River Basin, with the highest elevation of 3846m and the lowest of 1337m, and the terrain is low in the south and high in the north. Influenced by the westerly wind belt, the climate in the basin is cold, and the lowest temperature can reach -50℃. Precipitation is mostly in the form of snow, and a stable snow season is formed in the basin from November to April, and a thick and stable snow layer is easily formed in winter, with a snow depth of more than 1m, and the snow in the mountainous areas at higher altitudes continues to melt gradually in June. The catchment area of the watershed is 2350 km^2, with the lowest precipitation in February and March. The surface vegetation of the watershed is low grassland, with forests covering the shaded and semi-shaded slopes of the river channel, while grassland and scrub are mainly found on the sunny and semi-sunny slopes.

III. Basin permafrost analysis model

III. A. Permafrost distribution and freezing number modeling

Permafrost is an important natural feature of the cryosphere, and it serves as an important link to the other components of the cryosphere. The types of permafrost can be categorized into short-term, seasonal and perennial

according to the length of time the soil remains frozen. As the global climate warms, the permafrost environment also changes significantly, which affects the distribution characteristics of permafrost and the area of perennial permafrost to different degrees. Globally, permafrost covers 25% of the total area, and the main development areas are Russia, Canada, China, the United States and northern Europe.

The current methods for modeling the active layer thickness are divided into two categories: based on physical processes and based on empirical statistics. In this paper, the freezing number model based on empirical statistics is chosen, which has been widely used in the Tibetan Plateau region.

The freezing number model quotes an F value to classify the permafrost type in a simple way, and the F value is used to determine whether the permafrost exists or not. When the F value is greater than 0.5, it proves that permafrost is distributed in this area. Conversely, when the F-value is less than 0.5, it means that no permafrost is developed in this region. The model only needs to input the surface temperature or air temperature, and then other parameters are calculated according to the model. And E=1 is a special case of the freezing number model. Namely:

$$F = \frac{\sqrt{DDF}}{\sqrt{DDF + E \cdot \sqrt{DDT}}} \tag{1}$$

$$\begin{cases} F > 0.5, \text{Multi-frozen soil} \\ F < 0.5, \text{Seasonal permafrost} \end{cases} \tag{2}$$

$$E = \sqrt{\frac{\lambda_t * Q_f}{\lambda_f * Q_t}} \tag{3}$$

In Eq. (1), DDF is the annual freezing index, DDT is the annual thawing index, and E is the adjustment parameter.

In Eq. (3), λ_f and λ_t are the thermal conductivity coefficients of frozen and thawed soils $\left(w \cdot m^{-1} \cdot {}^{\circ}C^{-1}\right)$, and Q_f and Q_t are the heat released when the rock and soil freezes and absorbed when the rock and soil thaws $\left(J \cdot m^{-3}\right)$, respectively.

The calculation of the value of F relies mainly on DDT, DDF with the parameter E, while the freezing and thawing indices are calculated using the Nelson method with the following formula and procedure:

$$\beta = \cos^{-1}\left(-\frac{T_a}{A}\right) \tag{4}$$

$$T_s = T_a + A\left(\frac{\sin\beta}{\beta}\right) \tag{5}$$

$$T_w = T_a - A\left(\frac{\sin\beta}{\pi - \beta}\right) \tag{6}$$

$$L_s = 365 \cdot \frac{\beta}{\pi} \tag{7}$$

$$L_w = 365 - L_s \tag{8}$$

$$DDT = T_s \cdot L_s \tag{9}$$

$$DDF = -T_w \cdot L_w \tag{10}$$

$$A = \frac{(T_{\max} - T_{\min})}{2} \tag{11}$$

where the annual mean surface temperature $\left({}^{\circ}C\right)$ is denoted by T_a. The annual surface temperature amplitude $\left({}^{\circ}C\right)$ is denoted by A.

III. B. Hydrologic Modeling of Permafrost in Watersheds

The SHAWDHM model is a product of coupling the distributed hydrological model GBHM2 model with the SHAW model as a framework.

GBHM2 is a grid-based slope model with fast computational efficiency and adapted to areas with complex terrain [21]. However, the hydrological calculation process on the slope cell is simplified and does not have cryospheric processes such as soil freeze-thaw and ice melt. On the other hand, the SHAW model is a one-dimensional land-surface simultaneous hydrothermal process model, which can explain the states of soil freeze-thaw, vegetation interception, evapotranspiration, and water transport, and is widely used to simulate the hydrothermal exchange between vegetation, snow, soil, and the atmospheric system (SVAT) [22], [23].

The SHAWDHM model absorbs the advantages of the two models and simulates the processes of soil freezing and thawing, sink production, and evapotranspiration at the watershed scale using the slope grid as the basic response unit. The model was developed and applied for the first time in the Upper Black River Basin and has been shown to have good simulation results.

III. B. 1) Spatial division of watersheds

In order to solve the topological problem and obtain more accurate sub-basin extents and connectivity relationships, the Pre GBHM program directly uses a high-resolution DEM for watershed delineation, and then upscales based on a resampling method to obtain a coarser-resolution grid for model calculations. The terrain within each grid is abstracted as a pair of geometrically symmetric rectangular slope cells, which are used as the basic units for model calculation.

In this paper, a DEM resolution of 96 m is used, and the Pre GBHM program resamples it to 100 m. The watershed delineation result outputs the river network parameters needed by the GBHM model, as well as the channel parameters and the grid row and column numbers within each sub-basin.

III. B. 2) Model Coupling Process

The hydrothermal simulation process of the SHAWDHM model is synchronized in both the vertical and slope sides. The vertical stratification of vegetation's, snow, dead leaves, and soil on the slope unit is performed in the SHAW model. On the basis of this stratification, a finite difference method is used to discretize the energy and water transport in the system in time and space, and a system of linear equations about the mutual coupling of water and heat is established. Taking soil as an example, the balance equations of energy and water are:

$$C_s \frac{\partial T}{\partial t} - \rho_i L_f \frac{\partial \theta i}{\partial z} = \frac{\partial}{\partial z}\left[\lambda \frac{\partial T}{\partial z}\right] - \rho_L C_L \frac{\partial q_L T}{\partial z} - L_v \left(\frac{\partial q_v}{\partial z} + \frac{\partial \rho_v}{\partial t}\right) \tag{12}$$

$$\frac{\partial \theta_L}{\partial t} + \frac{\rho_i}{\rho_L}\frac{\partial \theta_i}{\partial t} = \partial\left[K\left(\frac{\partial \psi}{\partial z} + 1\right)\right] + \frac{1}{\rho_L}\frac{\partial q_v}{\partial z} + U \tag{13}$$

where T, ψ, θ_L, and θ_i are the soil temperature $\left(^{\circ}C\right)$, soil water potential (m), liquid water content, and ice content (%), respectively. t is the time (s), z is the depth (m) at each node, and C_S and C_L are the heat capacities of the soil and water, respectively $\left(J \cdot kg^{-1} \cdot s^{-1}\right)$. ρ_L, ρ_i, and ρ_v are the densities $\left(kg \cdot m^{-3}\right)$ of water, ice, and water vapor, respectively, and L_f and L_v are the heats of melting and vaporization, respectively. q_L, q_v, λ, K, and U are the flux of water $\left(m \cdot s^{-1}\right)$, the flux of water vapor $\left(kg \cdot m^{-2} \cdot s^{-1}\right)$, the thermal conductivity $\left(W \cdot m^{-1} \cdot {}^{\circ} C^{-1}\right)$, and the hydraulic conductivity $\left(m \cdot s^{-1}\right)$ and the source-sink term $\left(m^3 \cdot m^{-3} \cdot s^{-1}\right)$.

Based on the moisture conditions and freeze-thaw state of each soil layer, Darcy's law is applied to calculate the infiltration of soil water at the lower boundary of the unsaturated zone to obtain the groundwater level, and baseflow qg is obtained by simulating the interaction of groundwater and river based on the slope groundwater level, river level, and the effect of soil freezing and thawing on the soil hydraulic conductivity. When the depth of soil freezing and thawing is deeper than the maximum soil thickness that can be expressed by the model, the model uses the simulated bottom-most soil temperature to drive Stefan's formula to calculate the freezing depth D_f of the submerged layer:

$$q_g(t) = K_g\left(1-\frac{D_f}{D_g}\right)\frac{H_1-H_2}{L/2}\cdot\frac{h_1+h_2}{2} \tag{14}$$

where q_g, K_g, D_f, and D_g denote the groundwater single-breadth discharge $\left(m^3\cdot m^{-1}\cdot s^{-1}\right)$, groundwater conductivity $\left(m\cdot s^{-1}\right)$, submerged layer freezing depth, and submerged layer thickness (m), and h_2 is the depth of river level, respectively. (m).

Calculate the surface storage (m) based on the surface yield already simulated by the model, and apply the one-dimensional power wave equation to calculate the slope diffusive flow $q_s\left(m^3\cdot m^{-1}\cdot s^{-1}\right)$ on each slope cell. The surface water storage is updated as the upper boundary condition for solving the moisture transport at the next moment. Utilizing the layered structure of the soil, calculate the mid-loam flow $q_{sub}\left(m^3\cdot m^{-1}\cdot s^{-1}\right)$ for each layer of the soil in terms of the freezing and thawing conditions, hydraulic conductivity, and other hydrodynamic parameters:

$$q_{sub} = \sum_{i}^{n} K_i \Delta z_i \sin\alpha \tag{15}$$

where i denotes the soil layer sequence, K_i is the hydraulic conductivity of the first i layer $\left(m\cdot s^{-1}\right)$, Δz_i is the soil thickness of the first i layer (m), α is the gradient of the slope unit, and n is the number of soil layers.

Slope diffuse flow, loamy center flow, and base flow on the slope unit all laterally recharge the stream in the corresponding flow zone, and the runoff volume of each stream segment is calculated using the power wave equation sequentially converging from the source of the stream to the outlet of the watershed, and the depth of the river level is updated. The power wave equation is:

$$\frac{\partial A}{\partial t}+\frac{\partial Q}{\partial x} = q \tag{16}$$

$$Q = \frac{S_0^{1/2}}{nP^{2/3}}A^{5/3} \tag{17}$$

where A is the cross-sectional area of the river $\left(m^2\right)$, x is the length along the direction of the river (m), $q = q_g + q_{sub} + q_s$ is the river's single-width lateral recharge $\left(m^3\cdot m^{-1}\cdot s^{-1}\right)$, t is the time (s), S_0 is the riverbed specific drop, Q is the river flow $\left(m^3\cdot s^{-1}\right)$, n is the Manning's roughness length, and P is the wetted perimeter of the riverbed (m).

The above process is computed iteratively in a loop within a time step.The overall flow of the SHAWDHM model can be shown in Fig. 1.

III. C. Model Input Data and Output Data

III. C. 1) Model input data

The SHAWDHM model is a distributed hydrological model for cold regions based on physical processes, and its operation requires a large number of input data and parameters, which mainly include: drive data set, topographic data set, river channel parameter set, vegetation and soil parameter set, initial and boundary condition data set, and other control parameter sets.

According to the time-varying characteristics input data can be further divided into static parameter sets and dynamic input data. The input data are mostly stored in spatial data format and lookup table format.

III. C. 2) Model output data

Data output from the SHAWDHM model includes the hydrothermal state within the SVAT system as well as the flow production and sinks in the watershed. Examples include internal soil data: soil temperature, soil moisture content and ice content, and mid-soil flow, as well as surface data: surface runoff, baseflow, evapotranspiration, snowpack temperature, and snowpack depth.

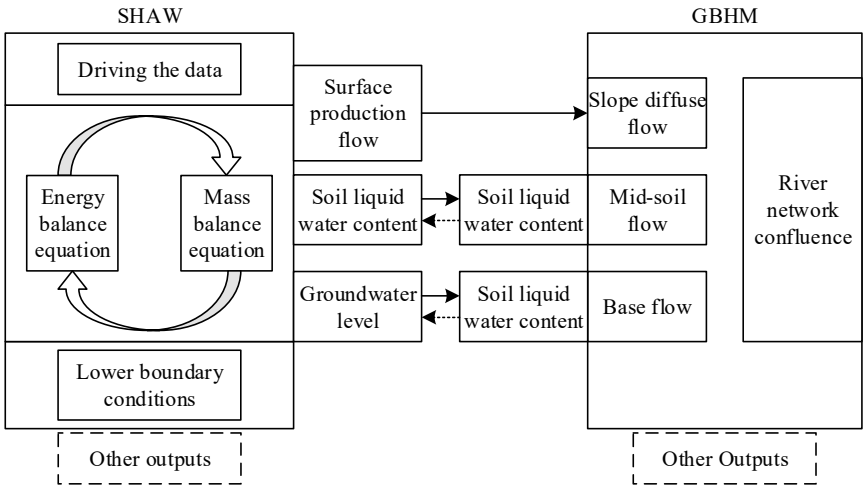

Figure 1: SHAWDHM model coupling flowchart

III. D. Analysis of hydrological changes in permafrost based on hydrological simulation results

III. D. 1) Indicators for analysis of permafrost processes

Permafrost exists in the form of perennial permafrost (also known as permafrost) and seasonal permafrost. Perennial permafrost refers to permafrost in which a frozen layer exists in the soil throughout the year. Seasonal permafrost, on the other hand, refers to a form of permafrost in which the frozen layer is formed by freezing during the cold season (or freezing season) and melts away during the warm season (or thawing season).

During permafrost degradation, the upper surface of the frozen layer of permafrost becomes progressively deeper (i.e., the active layer becomes progressively deeper), while the lower surface becomes progressively shallower. As the degradation gradually intensifies, the upper and lower surfaces of the frozen permafrost layer come into contact and the frozen layer disappears completely, i.e., the permafrost is degraded to seasonal permafrost. After that, as the temperature continues to rise, the thickness of the frozen layer of seasonal permafrost in the freezing season will also continue to become shallower, including at the same time the continued deepening of the upper surface of the frozen layer and the gradual shallowing of the lower surface (i.e., the freezing depth of seasonal permafrost).

In this paper, three indicators are selected to represent and measure the degradation level of permafrost, which are the proportion of perennial permafrost area in the watershed, the thickness of perennial permafrost active layer and the maximum freezing depth of seasonal permafrost.

(1) Proportion of perennial permafrost area

The proportion of perennial permafrost area reflects the spatial distribution characteristics of permafrost in the basin. The analysis of the spatial distribution of permafrost and seasonal permafrost can obtain the spatial distribution conditions of permafrost in different watersheds, the elevation of the junction between permafrost and seasonal permafrost, and the vegetation and hydrological conditions of different permafrost areas. Clarifying the spatial distribution of permafrost in watersheds is important for further analyzing the influence of permafrost changes on hydrological processes.

Changes in the proportion of perennial permafrost area characterize the degradation process from perennial permafrost to seasonal permafrost and the degradation rate, which is one of the most important elements to characterize the degradation rate of permafrost in the basin. Based on the comparison of the spatial distribution of permafrost in different ages, we can get the area of the basin where permafrost degrades to seasonal permafrost, and then we can analyze the hydrological changes in the area of permafrost degradation, so as to explore the influence of the degradation of permafrost on the hydrological process in depth.

(2) Thickness of active layer of permafrost

In the permafrost area, the most important index that characterizes the change of permafrost is the change of active layer thickness. The thickening of the active layer thickness reflects the degradation of permafrost, and its thickening rate characterizes the rate of permafrost degradation in the permafrost zone. Changes in the thickness of the active layer of permafrost will affect changes in the water storage capacity of permafrost soils, which in turn will affect the soil moisture in the watershed. Therefore, in-depth understanding of the changes in the thickness of the active layer is very important for analyzing the changes in permafrost in the watershed and its impact on hydrological processes.

(3) Maximum freezing depth of seasonal permafrost (MTSFG)

In seasonal permafrost areas, the concept of permafrost “active layer” does not exist because permafrost completely melts during the thawing season. In this case, the maximum frozen depth of seasonal permafrost is the most important indicator to characterize permafrost changes. Since most of the national weather stations are established in seasonal permafrost areas, and soil freezing depth (and soil temperature) is also observed at the weather stations, many previous studies have been based on the change of the maximum freezing depth of seasonal permafrost to characterize the change of permafrost.

III. D. 2) Analysis of changes in hydrological processes in the basin

Changes in hydrological processes in the watershed are analyzed based on the results of runoff, evapotranspiration, soil water, and water balance simulated by the SHAWDHM model. Among them, the focus is on analyzing the changes in annual runoff and evapotranspiration in the watershed, the changes in soil water, and the changes in the water balance of the watershed, in order to pave the way for the subsequent study of the effects of permafrost on hydrological processes.

(1) Annual runoff and ET volume

(2) Water balance of the watershed

(3) Soil moisture

IV. Changes in permafrost hydrology based on distributed hydrological modeling results

IV. A. Characterization of changes in permafrost

IV. A. 1) Inter-annual variation in area of distribution

Climate is the most important driver of permafrost environmental change. Influenced by regional climate warming, the permafrost environment changes significantly.

In order to study the interannual trend of perennial permafrost planar distribution, the distribution area of perennial permafrost from 1990 to 2022 was counted.The change in the proportion of the distribution area of perennial permafrost in the upper reaches from 1990 to 2022 is shown in Fig. 2.

The proportion of the distribution area of permafrost in 1990-2022 shows a clear downward trend, indicating that there is a relatively obvious degradation trend of permafrost, and the average degradation rate is about 1%/a.

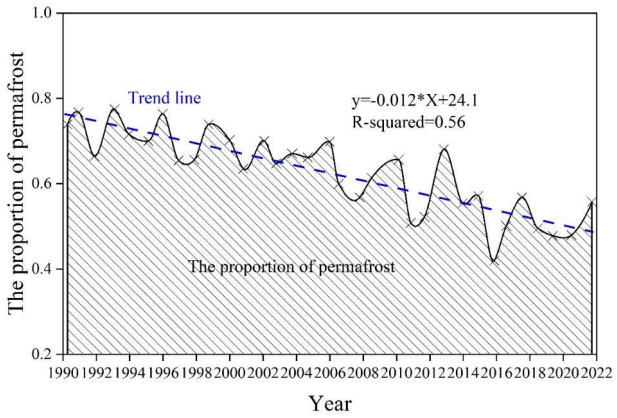

Figure 2: The proportion of permafrost distribution in the upstream years of 1990-2022

IV. A. 2) Changes in the lower boundary of permafrost

The lower boundary of perennial permafrost is usually considered to be the line of lowest elevations of the island perennial permafrost. To reflect the inter-annual variability of permafrost in the vertical direction, the lower boundary mean elevation of permafrost was used for the analysis.

The statistics of the multi-year changes in the mean elevation of the lower boundary of the perennial permafrost in the study area are shown in Figure 3, where the mean elevation of the lower boundary of the perennial permafrost showed an increasing trend from 1990 to 2022, with an increase rate of 10 m/a.

The lower boundaries of permafrost in 1994, 2004, 2014, and 2020 were about 3400 m, 3515 m, 3650 m, and 3745 m. The lower boundaries of permafrost in 2021 began to show a decreasing trend.

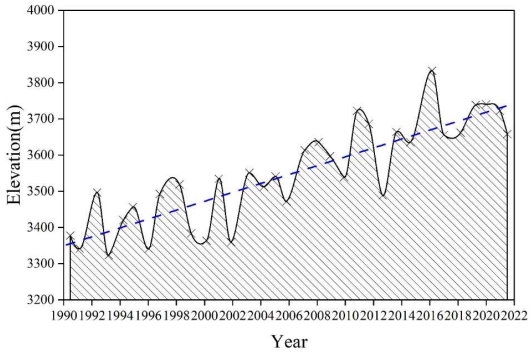

Figure 3: The study of the average height of the frozen permafrost in the region for years

IV. A. 3) Changes in the distribution of permafrost

In order to analyze the relative change in the area of multi-year freeze distribution at a given time period, the years 1990 to 2022 were divided into eight time periods, namely 1990 to 1994, 1995 to 1998, 1999 to 2002, 2003 to 2006, 2007 to 2010, 2011 to 2014, 2015 to 2018, and 2019 to 2022 Year. Based on the annual mean surface temperature and amplitude of each time period to find the distribution of permafrost in each time period, statistics of the change of the area of permafrost distribution in two adjacent time periods.

The change types of permafrost in the two time periods were categorized into four types, which were new perennial permafrost, degraded perennial permafrost, seasonal permafrost, and perennial permafrost. Among them, perennial permafrost and seasonal permafrost are those permafrost types that remain relatively stable for a long period of time. New permafrost is permafrost that changes from seasonal permafrost in the previous time period to permafrost in the subsequent time period. Degraded permafrost means seasonal permafrost that has changed from permafrost in the previous time period to permafrost in the subsequent time period. Both new and degraded permafrost are concentrated in areas where seasonal permafrost transitions to perennial permafrost, mostly in the West Branch of the watershed.

The statistics of the distribution area of the four types of permafrost between time periods from 1990 to 2022 are shown in Table 1.

The additional permafrost occurs in the 1995~1998 to 1999~2002, 2003~2006 to 2007~2010, and 2015~2018 to 2019~2022 changes, with an area of $0.002\times10^4 km^2$, $0.042\times10^4 km^2$, $0.001\times10^4 km^2$. In addition, the area of degraded permafrost is 0.005~$0.102\times10^4 km^2$. Which remained relatively stable from 1990 to 2022.

The areas of perennial permafrost distribution are $0.781\times10^4 km^2$, $0.712\times10^4 km^2$, $0.658\times10^4 km^2$, 0.665 $times10^4 km^2$, $0.604\times10^4 km^2$, $0.543\times10^4 km^2$, $0.467\times10^4 km^2$, showing a clear decaying trend.

Overall, the planar distribution of perennial permafrost degraded significantly from 1990 to 2022, and the newly added and degraded permafrost were located in the area of transition from seasonal to perennial permafrost, and mainly in the western branch of the upper part of the study basin.

Table 1: The distribution of four frozen permafrost in different time periods ($\times10^4 km^2$)

Time sequence	Permafrost	Degraded permafrost	Seasonal permafrost	Permafrost
1990~1994 1995~1998	0	0.005	0.214	0.781
1995~1998 1999~2002	0.002	0.002	0.321	0.712
1999~2002 2003~2006	0	0.0035	0.318	0.658
2003~2006 2007~2010	0.042	0.0079	0.349	0.665
2007~2010 2011~2014	0	0.001	0.387	0.604
2011~2014 2015~2018	0	0.0102	0.384	0.543
2015~2018 2019~2022	0.001	0.07	0.503	0.467

IV. B. Changes in permafrost hydrology

(1) Changes in seasonal permafrost maximum freezing depth and perennial permafrost active layer thickness

The changes in the perennial permafrost active layer thickness and seasonal permafrost maximum freezing depth in the study area from 1968 to 2022 are shown in Fig. 4.

From the figure, it can be seen that the annual average of the thickness of the active layer of perennial permafrost in the study area shows a clear increasing trend, rising at a rate of 0.012 m/10a. The annual mean maximum freezing depth of seasonal permafrost shows a clear decreasing trend with a rate of change of 0.07 m/10a.This result indicates that the change in maximum freezing depth of seasonal permafrost in the study area is more drastic than the change in the thickness of the active layer of multi-year permafrost. The above results also indicate that significant degradation of both perennial and seasonal permafrost has occurred in the source area of the Irtysh River Basin during the past 54 years.

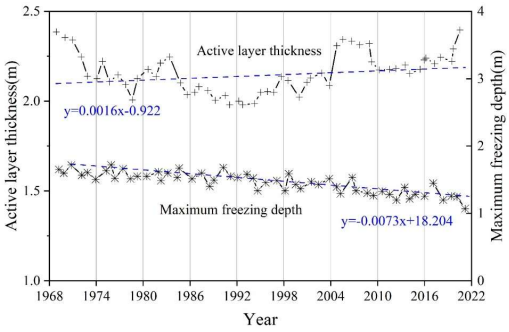

Figure 4: 1968-2022 study of regional permafrost

(2) Groundwater recharge

Based on the analysis of the data on land use types in the upper part of the source area of the Irtysh River Basin, and the relatively few behaviors such as farm irrigation and anthropogenic mining in the source area, groundwater recharge is considered to be the soil infiltration, which is the vertical water flux from the bottom of the encompassing zone that is replenished to the submerged surface.

The SHAWDHM model calculates this flux from soil moisture at the bottom of the unsaturated zone to the water table using Darcy's law.The relationship between simulated soil infiltration, measured 20% annual precipitation, and the proportion of perennial permafrost area to the total area of the watershed for the years 1972-2022 for SHAWDHM is shown in Fig. 5 from year to year.

It can be seen that the curve of the ratio of perennial permafrost to watershed area shows a decreasing trend in 1996 and decreases to 27% in 2022. The annual soil infiltration curve is lower than the 20% annual precipitation curve during the observation period. However, around 2018, the annual soil infiltration curve is slightly higher than the 20% annual precipitation curve.

The percentage of perennial permafrost area fluctuated above and below 35% from 1972 to 1996, and the changes in soil infiltration obtained from the simulation were mainly influenced by the changes in precipitation.

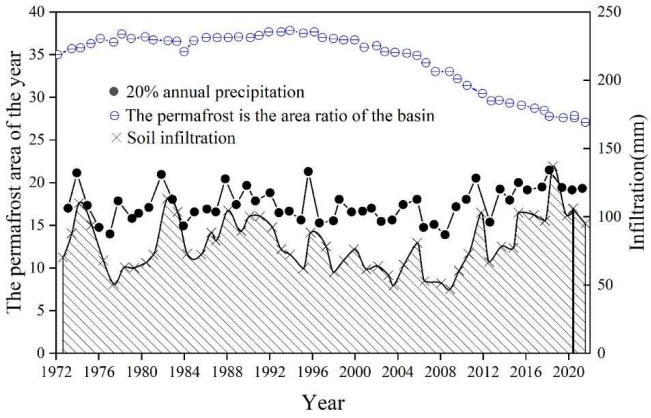

Figure 5: The results of the SHAWDHM simulation in 1972-2022

A comparison of SHAWDHM simulated soil infiltration with measured precipitation is shown in Figure 6.

Simulated soil infiltration was relatively low from 1976-1980, and soil infiltration increased rapidly from 1982-1983, corresponding to an increase in precipitation.Soil infiltration showed a decreasing trend from 1988-1996, associated with a decrease in precipitation.

After 2008, soil infiltration increased rapidly with warmer temperatures and increased soil hydraulic conductivity, without a significant increase in precipitation.

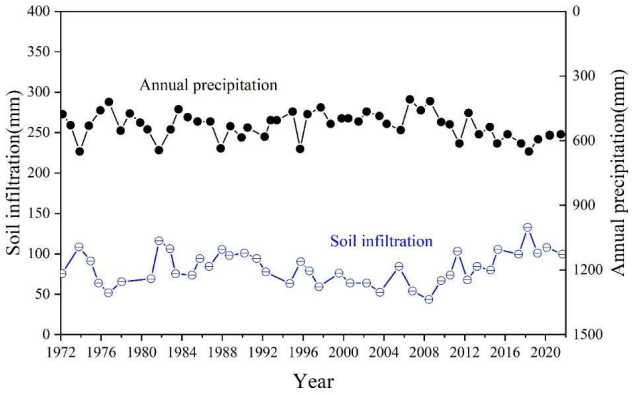

Figure 6: The soil infiltration is compared with the measured precipitation

V. Conclusion

This paper analyzes the general situation of the Irtysh River basin, combines the actual situation of the upstream of the source area of the Irtysh River basin, and uses the model SHAWDHM to simulate the year-by-year changes in the relationship between the amount of soil infiltration, 20% of the annual precipitation, and the proportion of the area of perennial permafrost to the total area of the basin.

(1) The proportion of the distribution area of perennial permafrost in the upstream of the source area of the Irtysh River Basin shows an obvious decreasing trend from 1990 to 2022.The lower boundary of perennial permafrost shows an increasing trend on average, reflecting a fluctuating upward trend, and the lower boundary of the upstream perennial permafrost will be about 3,660 m in 2022.The degradation of the planar distribution of the perennial permafrost from 1990 to 2022 is significantly, the new permafrost and degraded permafrost are located in the area of transition from seasonal permafrost to perennial permafrost, and are mainly located in the west branch of the upper reaches of the study basin.

(2) From 1968 to 2022, the annual mean of the thickness of the active perennial permafrost layer in the headwaters of the Irtysh River Basin shows a significant increasing trend, rising at a rate of 0.012 m/10a. The annual mean maximum freezing depth of seasonal permafrost showed a significant decreasing trend, with a rate of change of 0.07 m/10a. Both perennial and seasonal permafrost underwent significant degradation. The percentage of perennial permafrost area fluctuated above and below 35% from 1972 to 1996, and the changes in soil infiltration obtained by the model SHAWDHM simulation were mainly affected by the changes in precipitation.

Funding

This study was supported by Special Project for the Construction of Innovation Environment in the Autonomous Region-Construction of Resource Sharing Platform (PT2323); The Third Xinjiang Scientific Expedition Program (Grant No.2021xjkk1300)"; Guided project of the Xinjiang Uygur Autonomous Region Meteorological Service (YD2022020).

References

[1] Chadburn, S. E., Burke, E. J., Cox, P. M., Friedlingstein, P., Hugelius, G., & Westermann, S. (2017). An observation-based constraint on permafrost loss as a function of global warming. Nature climate change, 7(5), 340-344.

[2] Koven, C. D., Ringeval, B., Friedlingstein, P., Ciais, P., Cadule, P., Khvorostyanov, D., ... & Tarnocai, C. (2011). Permafrost carbon-climate feedbacks accelerate global warming. Proceedings of the National Academy of Sciences, 108(36), 14769-14774.

[3] Huang, F., Xia, Z., Li, F., Guo, L., & Yang, F. (2012). Hydrological changes of the Irtysh River and the possible causes. Water resources management, 26, 3195-3208.

[4] Ding, Y., Zhang, S., Zhao, L., Li, Z., & Kang, S. (2019). Global warming weakening the inherent stability of glaciers and permafrost. Science bulletin, 64(4), 245-253.

[5] Biskaborn, B. K., Smith, S. L., Noetzli, J., Matthes, H., Vieira, G., Streletskiy, D. A., ... & Lantuit, H. (2019). Permafrost is warming at a global scale. Nature communications, 10(1), 264.

[6] Liu, L., Zhao, D., Wei, J., Zhuang, Q., Gao, X., Zhu, Y., ... & Zheng, D. (2021). Permafrost sensitivity to global warming of 1.5 C and 2 C in the Northern Hemisphere. Environmental Research Letters, 16(3), 034038.
[7] Grosse, G., Goetz, S., McGuire, A. D., Romanovsky, V. E., & Schuur, E. A. (2016). Changing permafrost in a warming world and feedbacks to the Earth system. Environmental Research Letters, 11(4), 040201.
[8] Dobiński, W. (2020). Permafrost active layer. Earth-Science Reviews, 208, 103301.
[9] Li, G., Zhang, M., Pei, W., Melnikov, A., Khristoforov, I., Li, R., & Yu, F. (2022). Changes in permafrost extent and active layer thickness in the Northern Hemisphere from 1969 to 2018. Science of The Total Environment, 804, 150182.
[10] Shen, T., Jiang, P., Ju, Q., Yu, Z., Chen, X., Lin, H., & Zhang, Y. (2023). Changes in permafrost spatial distribution and active layer thickness from 1980 to 2020 on the Tibet Plateau. Science of The Total Environment, 859, 160381.
[11] Wu, Q., Zhang, T., & Liu, Y. (2012). Thermal state of the active layer and permafrost along the Qinghai-Xizang (Tibet) Railway from 2006 to 2010. The Cryosphere, 6(3), 607-612.
[12] Luo, D., Wu, Q., Jin, H., Marchenko, S. S., Lü, L., & Gao, S. (2016). Recent changes in the active layer thickness across the northern hemisphere. Environmental Earth Sciences, 75, 1-15.
[13] Peng, X., Zhang, T., Frauenfeld, O. W., Mu, C., Wang, K., Wu, X., ... & Luoto, M. (2023). Active layer thickness and permafrost area projections for the 21st century. Earth's Future, 11(8), e2023EF003573.
[14] Wu, Q., Hou, Y., Yun, H., & Liu, Y. (2015). Changes in active-layer thickness and near-surface permafrost between 2002 and 2012 in alpine ecosystems, Qinghai–Xizang (Tibet) Plateau, China. Global and Planetary Change, 124, 149-155.
[15] You, Y., Guo, L., Yu, Q., Wang, X., Pan, X., Wu, Q., ... & Wang, G. (2022). Spatial variability and influential factors of active layer thickness and permafrost temperature change on the Qinghai-Tibet Plateau from 2012 to 2018. Agricultural and Forest Meteorology, 318, 108913.
[16] Zhao, D., & Wu, S. (2019). Projected changes in permafrost active layer thickness over the Qinghai-Tibet Plateau under climate change. Water Resources Research, 55(9), 7860-7875.
[17] Li, R., Zhao, L., Ding, Y., Wu, T., Xiao, Y., Du, E., ... & Qiao, Y. (2012). Temporal and spatial variations of the active layer along the Qinghai-Tibet Highway in a permafrost region. Chinese Science Bulletin, 57, 4609-4616.
[18] Zhao, L., Wu, Q., Marchenko, S. S., & Sharkhuu, N. (2010). Thermal state of permafrost and active layer in Central Asia during the international polar year. Permafrost and Periglacial Processes, 21(2), 198-207.
[19] Faucherre, S., Jørgensen, C. J., Blok, D., Weiss, N., Siewert, M. B., Bang-Andreasen, T., ... & Elberling, B. (2018). Short and long-term controls on active layer and permafrost carbon turnover across the Arctic. Journal of Geophysical Research: Biogeosciences, 123(2), 372-390.
[20] Hrbáček, F., Oliva, M., Hansen, C., Balks, M., O'Neill, T. A., de Pablo, M. A., ... & Lacelle, D. (2023). Active layer and permafrost thermal regimes in the ice-free areas of Antarctica. Earth-Science Reviews, 242, 104458.
[21] W. Wang,H. Lu,B. Gao,Y. Jiao & Z. Pang. (2015). Simulating hydrological processes in a sub-basin of the Mekong using GBHM and RS data. Proceedings of the International Association of Hydrological Sciences,368(368),221-226.
[22] Jing Xue,Chong Fu,Junfeng Chen & Lihong Cui. (2025). Evaluating the influence of different straw mulch-autumn irrigation patterns on soil water, heat, and salt in seasonally frozen regions with distributed SHAW model. Agricultural Water Management,311,109377-109377.
[23] Lifeng Zhou,Hao Zhang,Liwang Ma,Kadambot H.M. Siddique & Hao Feng. (2025). Simulating plastic mulching effects on the soil water balance and maize yields using the modified RZ-SHAW model. Field Crops Research,322,109712-109712.